IEEE Access
Multidisciplinary | Rapid Review | Open Access Journal

Received January 31, 2021, accepted February 27, 2021, date of publication March 8, 2021, date of current version March 16, 2021.

Digital Object Identifier 10.1109/ACCESS.2021.3064348

A Quad-Band Stacked Hybrid Ambient RF-Solar Energy Harvester With Higher RF-to-DC Rectification Efficiency

SUNANDA ROY[1], (Graduate Student Member, IEEE), JUN-JIAT TIANG[1], MARDENI BIN ROSLEE[1], (Senior Member, IEEE), MD TANVIR AHMED[1], (Student Member, IEEE), AND M. A. PARVEZ MAHMUD[2]

[1]Faculty of Engineering (FOE), Multimedia University, Cyberjaya 63000, Malaysia
[2]School of Engineering, Deakin University, Geelong, VIC 3216, Australia

Corresponding author: Sunanda Roy (sunandaroy75@gmail.com)

This work was supported in part by the TM Research and Development Research, Malaysia, under Grant MMUE/190001.02.

ABSTRACT This article addresses the design and implementation of a novel quad-band electromagnetic (EM) and solar energy scavenging system, ensuring energy harvesting from ambient RF environment with excellent ''cold start'' power level. The proposed scavenger consists of a single port quad-band rectangular slot antenna, power film solar cell, a quad-band RF- to-DC converter, a microcell power management module, and a battery. The harmonic balance of EM solver is used to design and maximize the RF- to - DC rectification efficiency with the combination of the antenna and the solar cell. The power film solar cell is placed in the middle of the antenna with positive and negative edges connected to the top and bottom layer of the antenna so that total harvested energy passes through the rectifier and forms an ambient hybrid energy harvesting system. One significant benefit of this method is the utilization of the antenna free space for the effective area of the power film. Another important contribution is the employment of multiband antennas for increasing the total ambient RF scavenged energy. Besides, a cost-effective and flexible FR4 substrate and a micropower film solar cell are used to make it conformal and cheaper. The prototype of hybrid harvester demonstrated that with 360 lux ambient light intensity, at the solar cell can generate 0.109 V energy while the harvester can attain an extra 5% - 48% energy with ambient RF input level variation from −15 to −20 dBm. The rectifier circuit achieves 74.5% RF-to-DC rectification efficiency for the value of load resistance 2.7 kΩ. These performances depict that the proposed multiband ambient hybrid RF-solar power scavenger can raise the scavenged power level and offer energy multiplicity.

INDEX TERMS Multiband, rectifier, hybrid harvester, power film solar cell, ambient RF, rectangular slot antenna.

I. INTRODUCTION

Finding the alternate use of battery for large scale wireless sensor node (LSWSN) has been a vital issue recently [1], radio frequency identification (RFID) system [2], Internet of Things (IoT) [3], health monitoring system (HMS) [4], smart skin sensors [5], to name a few. To fulfil this demand, many researchers are suggesting various techniques to harvest energy (RF / solar) from the ambient environment (indoor or outdoor) and converting it into DC energy [6]. Various energy sources from various environments are available for scavenging energy such as radio frequency (RF) electromagnetic (EM) waves [7]–[11], sunlight [12], vibration [14], and many other forms of kinetic and thermal energy [13]. Solar energy is considered as one of the largest ambient energy sources which offer sufficient power from its light. When illuminated using the normal global solar irradiance spectrum corresponding to air mass 1.5 (AM1.5 G) and at T=25^0, also known as 1 Sun= 100 milliwatt (mW)/cm^2, the usual power levels that solar cells considered in this work can provide are in the

The associate editor coordinating the review of this manuscript and approving it for publication was Rami Ghannam.

order of mW [15]. In cloudy environments, the illuminated power level drops to microwatt (μW). These freely available energy sources are frequently transient and RF power levels randomly vary which restricts the reliability of the scavenged energy level. The energy conversion efficiency is another challenging issue for the power harvesting approach from very low-level RF power associated with fabricated materials for 3rd generation power film solar cells [16]. Besides, overall research objects are cost-effective and efficient power film solar cells design can perform maximum power point tracking (MPPT) to boost the solar harvesting process using low-level DC / DC energy conversion technique [12], [17], [18]. To overcome these limitations, a multiband hybrid energy scavenger is proposed to extend the diversity of energy (RF and solar) harvesting approach. The multiband electromagnetic and solar energy scavenger is a combination of both solar power and rectenna systems combining for a simultaneous and uninterrupted approach of energy scavenging. Besides, solar energy scavenger offers higher DC output power with high-intensity irradiation of light from ambient environments.

The available RF energy level in the ambient environment is comparatively lower than solar energy. Moreover, RF-to-DC energy conversion rectifier circuits [19] permit wireless energy transmission and the ability to energize the lowest start-up power sensors using a cost-efficient transmitter [7]. The application of electromagnetic energy scavengers is directly supported by antennas that are capable of operating in an ambient wireless environment. The antenna is not only used for wireless communications but also widely used in EM energy scavenging technology. Consequently, the RF energy harvesting technology has become a more interesting research topic in recent times [8]. Due to the freely available and random variable ambient RF power sources, multiband hybrid harvesting techniques are essential to supply the required energy to operate small power electronic devices [20].

The proposed multiband antenna is designed in such a way that solar cell power film shares the same area of the antenna and integrates with radiator elements avoiding the degradation of antenna performance. The amorphous silicon solar cell is easily integrated with any type of antenna, especially the textile antenna [21]. This 2nd generation power film solar cell consists of hydrogenated silicon (Si: H) and can maximize DC power conversion efficiency (i.e. at least 10%) under 1 sun (100 mW/cm^2) illumination. The main objective of this work is to design and implement a realistic multiband ambient hybrid (RF / solar) energy harvester, in addition, to motivate more cost-effective, compact and flexible design to fulfil future demand. The voltage multiplier diode-based rectifier circuit is a type of Greinacher circuit that has been widely explored in the articles [22], [23]. Instead of focusing on the mutual nonlinear and EM optimization of the novel input impedance matching network (IMN), this research is based on the load label of a dual diode multiband rectifier circuit for freely available low RF power. It has better quad-band and broadband performance and uses flexible, solvent-free fabrication with the low-cost FR4 substrate material. The amount of harvested energy is really low in a cloudy environment which is approximately in the order of nanowatt (nW). This amount is high (i.e. in the order of mW) in high-density illuminated conditions. That means when the transition of light does not appear in a fully illuminated condition, the harvested power level is abruptly down. These harvested power levels are feasible in devices or systems such as various IoT and Embedded sensors that operate on very low duty cycles. This multiband electromagnetic and solar energy harvester has an advantage compared to single-band harvester generating higher power levels for future requirements. The key focus in this work is the hybrid harvester being able to harvest energy simultaneously from both low-level RF signals as well as solar irradiation.

In this work, we investigate three crucial attributes capable of the integration of micropower film solar cells with printed wide-slot antenna for applications of electromagnetic and solar energy harvesting approach. Firstly, the suggested fork-shaped slotted antenna provides large impedance bandwidth (BW) due to its additional fine-tuning capabilities and resonant modes respectively. The antenna has achieved 85% efficiency by integrating and sharing the same space as the solar cell. Secondly, a dual diode voltage multiplier quad-band rectifier circuit is designed, and the associated nonlinear behaviour is analyzed with the EM optimization technique for the low-level RF input. The suggested rectifier can achieve 79% RF-to-DC rectification efficiency for multiple RF tones with low-level signal power. Thirdly, the complete harvester is realized by integrating ultra-low-power boost converter BQ 25504, which has dynamic MPPT properties to harvest energy continuously from randomly variable low power input sources. The proposed hybrid harvester (antenna + rectifier) prototype is fabricated and measured the performance parameter in the lab. Measurement results demonstrate that harvested dc output power varies from 0.165 to 1.5 mW for non-irradiance and irradiance lighting conditions respectively while the ambient RF power varies from 14.50 to 53.50 mW/m^2. Furthermore, experimental results indicate that the scavenged dc power from multiband hybrid harvester is far better when a solar cell power film is integrated along with the antenna in a fully irradiated condition (higher density illumination of 360 lux). The suggested multiband electromagnetic and solar energy scavenger signifies the benefits of energy diversity in ambient applications. One potential approach is the integration of several sources of environmental energy harvesting to overcome the key challenges of RF energy harvesting by taking advantage of the specific features of additive manufacturing. In particular, this study proposes that RF and solar energy harvesters be hybridized into modules/topologies that can be assembled using additive manufacturing technology. In addition, this paper deals with an overview of the proposed hybrid RF solar energy harvesting system, the configuration and preliminary measurements of the antenna and rectifier, the results of the

preliminary module-level operation and the benchmarking of the hybrid harvester compared to the previously mentioned RF/solar energy harvesters.

This article is organized as follows. Section II depicts a brief literature review about hybrid energy harvester. Section III presents practical measurement of RF survey and solar power in ambient condition. Section IV describes the design and implementation of antenna as well as simulated and measurement results. Section V describes the integration of solar cell power film and effect on antenna performance. Section VI presents the design and implementation of quad-band rectifier and simulated and measured performances. Section VII describes the experimental setup and measurement in lab. Section VIII describes the effect of harvester performance using BQ-25504 EVM. Finally, this exploration is concluded in Section IX.

II. PRACTICAL RF SPECTRAL SURVEY AND SOLAR POWER MEASUREMENT

To realize available RF power levels exist in the ambient environment (i.e. urban, rural and semi-urban) in Malaysia, the RF spectral survey is performed within the frequency range (0.5-3 GHz) which is a part of the ultra-high frequency spectrum. Due to different types of propagation losses such as absorption path loss, multipath fading, refraction, diffraction and the number of base-stations in rural and urban areas, RF surveys do not provide exact information (available frequency ranges, power density level).

The multimedia university (MMU) in the semi-urban area is chosen to conduct RF surveys. The daytime is selected to measure the available ambient RF power and frequency level. A TTi PSA6005 spectrum analyzer with a calibrated 1.8 GHz isotropic antenna was used to measure electric field strength within the 0.5 GHz to 3 GHz frequency range. The selected antenna is tilted in orthogonal directions such that the spectrum analyzer records maximum reading. For every recording, more than 1.5 minutes is assigned to capture the best reading in a specific frequency band. The setting in the spectrum analyzer ensures the expected reading of power levels from non-dedicated RF sources in semi-urban environments. Figure 1 displays the measured available frequency bands such as GSM 900, GSM 1800, 3G, Wi-Fi and LTE and associated RF power density level. TABLE 1 depicts the

TABLE 1. Measured average RF power and frequency level.

Brand name	Freq. Range MHz)	Max. Power (dBm)
GSM 900 (M_{TX})	880 - 915	-27.6
GSM 900 (B_{TX})	925 - 960	-22.5
GSM 1800 (M_{TX})	1710-1785	-31.5
GSM 1800 (B_{TX})	1805-1880	-17.8
3G (M_{TX})	1920-1980	-27
3G (B_{TX})	2110-2230	-23
	2300-2360	-41.2
Wi-Fi	2390-2400	-25.6
LTE	2500-2700	-26.5

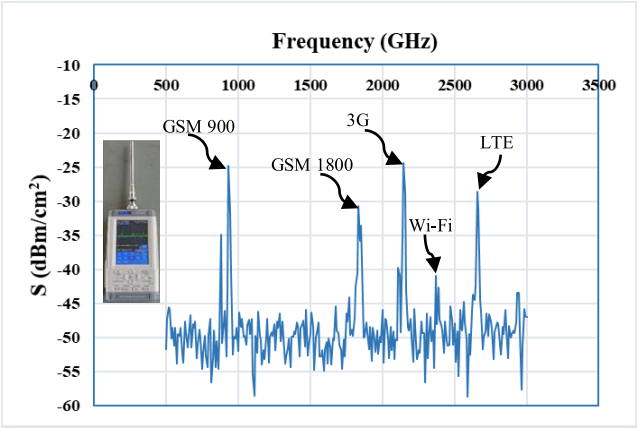

FIGURE 1. Measurements of RF power and frequency range.

numerical value of available frequency bands and associated RF input measurements. A high sensitive rectenna (antenna + rectifier) should be able to harvest energy over available frequency bands and associated input RF power density level.

The solar meter IM 750 is used to measure the solar power for different ambient temperatures (TABLE 2). These measurements (RF and solar) are properly utilized to design high sensitive multiband rectenna and identify the proper location where the harvester operated efficiently.

TABLE 2. Measured solar power in different ambient conditions.

Temperature (^{0}C)	26	27.5	28	29	30	34
Irradiance (W/m^2)	0.8	47.5	67.7	138.8	233	345.5

III. BROADBAND ANTENNA DESIGN

The designated printed wide-slot antenna with a rectangular shape is depicted in Figure 2. Both sides (top and bottom) of the designs are improved by a simple slot rectangular antenna with a fork-shaped stub. For a simple printed wide slot antenna with a rectangular structure connected to a fork-shaped tuning stub, the centre cut a rectangular slot and the fork-shaped linked feeding line is designed on top and sides of the selected dielectric material. The designed antenna is printed on an FR4 dielectric substrate, the dimension of 160 mm × 150 mm × 1.6 mm, dielectric constant (ε_r) of 5.4, and the loss tangent is 0.02. The size of the bottom slot is 121 mm × 121 mm. Figure 2 (a), (b) and (c) show the parametric dimensional details of the proposed antenna as well as the front and back side image of the fabricated antenna prototype respectively. TABLE 3 shows the final optimized dimension of various parameters of the proposed antenna structure. For best performance and maintaining the 50 Ω input impedance of the antenna, all parameters are optimized by computer simulation technology (CST v 18). The rectangular corners of the ground slot are replaced by round corners that ensure the smooth transition and improves impedance matching [24]. The antenna is designed to operate available frequency bands within 500 MHz to 3 GHz.

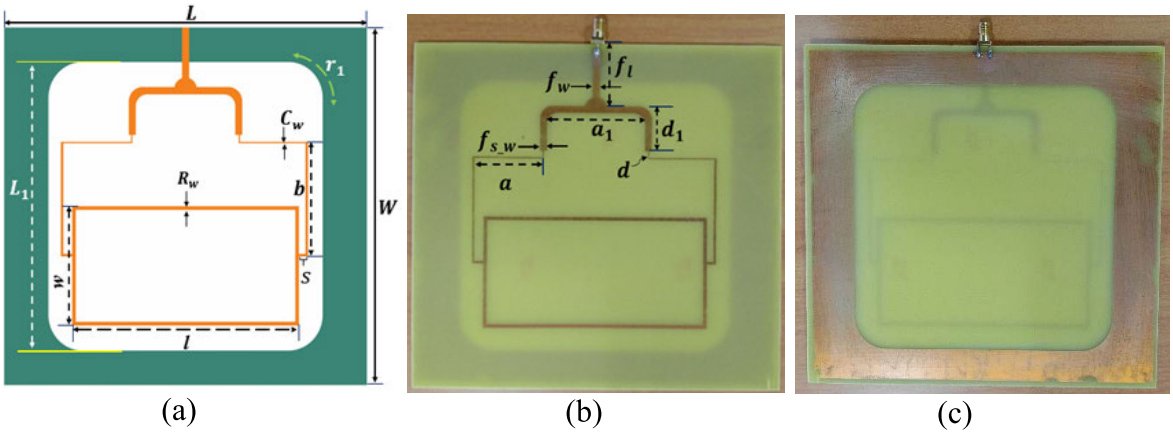

FIGURE 2. The proposed antennas (a) dimensional details, (b) prototype fabricated image font side, (c) prototype fabricated image back side.

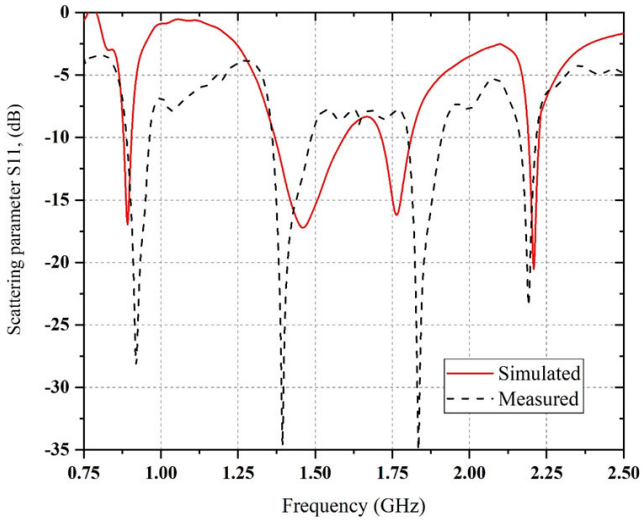

FIGURE 3. The comparison between the simulated and measured S-parameter of the proposed antenna.

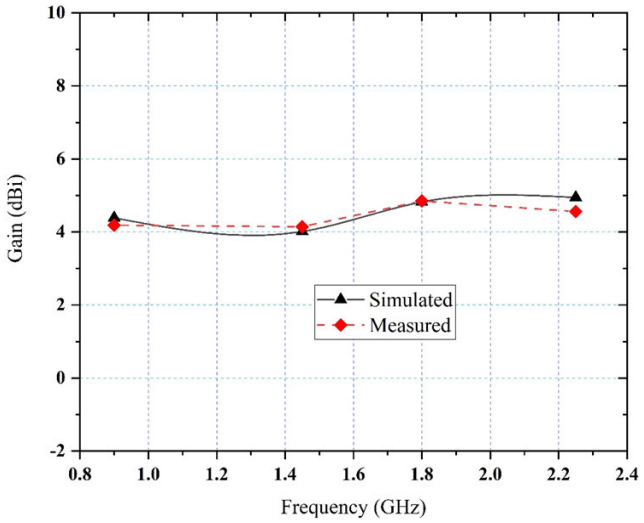

FIGURE 4. The comparison between simulated and measured realized peak gain.

It is observed that the first resonant frequency band is about GSM 900. The fork-shaped stub of the rectangular slot develops a broad impedance BW. The printed wide-slot antenna is integrated with a fork-shaped tuning stub which excites the multiple resonant modes. The appropriate dimension and position of the tuning stub, the intersection and impedance matching of selected multiple resonances can be boosted to get the wider impedance BW. The width of the leg of the fork-shaped stub determines the resonance frequency, higher width leads the higher resonance and lower width leads to the lower resonance frequency. To realize the parametric effect on the impedance bandwidth exhaustively, the investigation is conducted. The various parameters (length, wide and position) of the stub, as well as rectangular slot, mainly determine the impedance bandwidth.

The scattering parameters (S11) of the printed wideband antenna are tested by a vector network analyzer (VNA), and the measured results are compared with the simulated results (Figure 3). The measured reflection coefficient (S11) of the wideband antenna is less than −10 dB for all resonance frequency bands. It is observed that the simulated result is in good agreement with the measured result except for some minor shift towards higher frequency regions for all resonance bands. Some inconsistencies (between the simulated and measured RL result) are due to some errors of sub-miniature (SMA) male connector soldering and fabrication. Due to the appropriate position of the stub and dimension of the ground slot, 140% of impedance BW in the range of (0.5 - 2.5 GHz) is upgraded from 100% (0.8-3 GHz). Figure 4 shows the comparison between the simulated and measured gain of the proposed antenna.

It is observed that gain in each frequency band is above 4 dBi from 0.5 to 3 GHz, and the simulated and measured peak realized gain is similar in comparison. The comparison (between simulated, measured, with solar cell) of E-field and H-field radiation pattern for different frequency bands (0.9 GHz, 1.45 GHz, 1.81 GHz and 2.25 GHz) are depicted in Figure 5. The simulated and measured radiation pattern

TABLE 3. The optimized dimension of the proposed antennas.

Dimensional details	Symbol	Parametric value (mm)
Substrate length	L	160
Substrate wide	W	160
Ground slot length or wide	L_1	121
Rectangular slot length	l	100
Rectangular slot wide	w	50
Width of the rectangular slot	R_w	2
Connected horizontal arm	a	30.5
Connected horizontal arm width	c_w	0.5
Connected vertical arm	b	48
Horizontal spacing	s	4
Vertical spacing	d	3.5
Fork-shaped wide	a_1	44
Fork-shaped arm length	d_1	17
Fork-shaped arm width	$f_{s,w}$	3
Length of feedline	f_l	15
Bending radius	r_1	15

of the wideband antenna is good in agreement other than some discrepancies. The E-field and H-field radiation patterns of the proposed antenna are expressed as a stable dipolar (YZ-plane), and an omnidirectional pattern (XZ-plane) respectively.

IV. GEOMETRY OF SOLAR CELL AND INTEGRATION WITH ANTENNA

The flexible and reliable hydrogenated amorphous silicon solar cell power film (Figure 6 (a) & (b)) is selected in this project. The integration of solar power film has a minimal effect on performance due to its small thickness of material layers as depicted in Figure 6 (c). The solar cell power film structure has the same standard as the available commercial solar power film as shown in Figure 6 and has an identical structure which was suggested in [25]. The ZnO layer is the topmost layer of the solar cell which extracts light from the sun. It acts as a photodiode (p-i-n junction) and function is generating free carriers (photon generation) [26]. The reflective layer consists of a mixture of aluminium (Al), silver (Ag) and Zinc oxide (ZnO) which has high emission properties. The back layer communicates to a polyamide substrate which is used for flexible electronics of its solubility properties. The lowest thickness of the polyamide substrate and high reflective properties of the aluminium layer may have the potential to affect antenna performance.

The constructional and elementary details of the solar cell power film is demonstrated in Figure 6 (a). This solar cell power film structure that is same to the one suggested in [25] updated according to the requirements of the purchased power film can be depicted in Figure 6(b). The chosen solar cell power film is integrated into the free space location of the wideband printed antenna using glue so that it has minimal effect on the antenna performance. The positive terminal of power film is connected to the top of the antenna element and the negative terminal to the ground plan. The measured scattering parameter of the printed antenna with and without solar cells is shown in Figure 7. It can be seen that the power film has a minor effect on antenna characteristic impedance (input impedance). The measured scattering parameters between integrated and non-integrated solar power film antennas are in good agreement except for some minor discrepancies. The s-parameter response for power film integrated antenna (resonance for 1.35 GHz and GSM 1800) is higher than the non-integrated power film antenna (resonance for 0.9 GHz and 2.2 GHz). The measured directivity radiation pattern in the polar form of the wideband antenna with and without solar cell power film for separate frequency bands is shown in Figure 8. It is observed that solar cell power film has a slight effect on printed antenna directivity depending on different resonance frequencies and may dominate to increase the level of cross-polarization. The radiation patterns of the printed antenna have a small shift when solar cell power film is integrated on top of the blank space of the antenna element. To realize the appearance of antenna multiples resonances, surface current distribution at different frequencies (i. e 0.9 GHz, 1.45 GHz, 1.81 GHz and 2.25 GHz) are resented in Figure 9.

It can be seen that maximum current particles come out at the top rectangular slot and fork stub together with consistent major current density at the feeding line when the resonance frequency is lower 2.4 GHz which verifies the suggested idea. This justifies the design of rectangular slot which

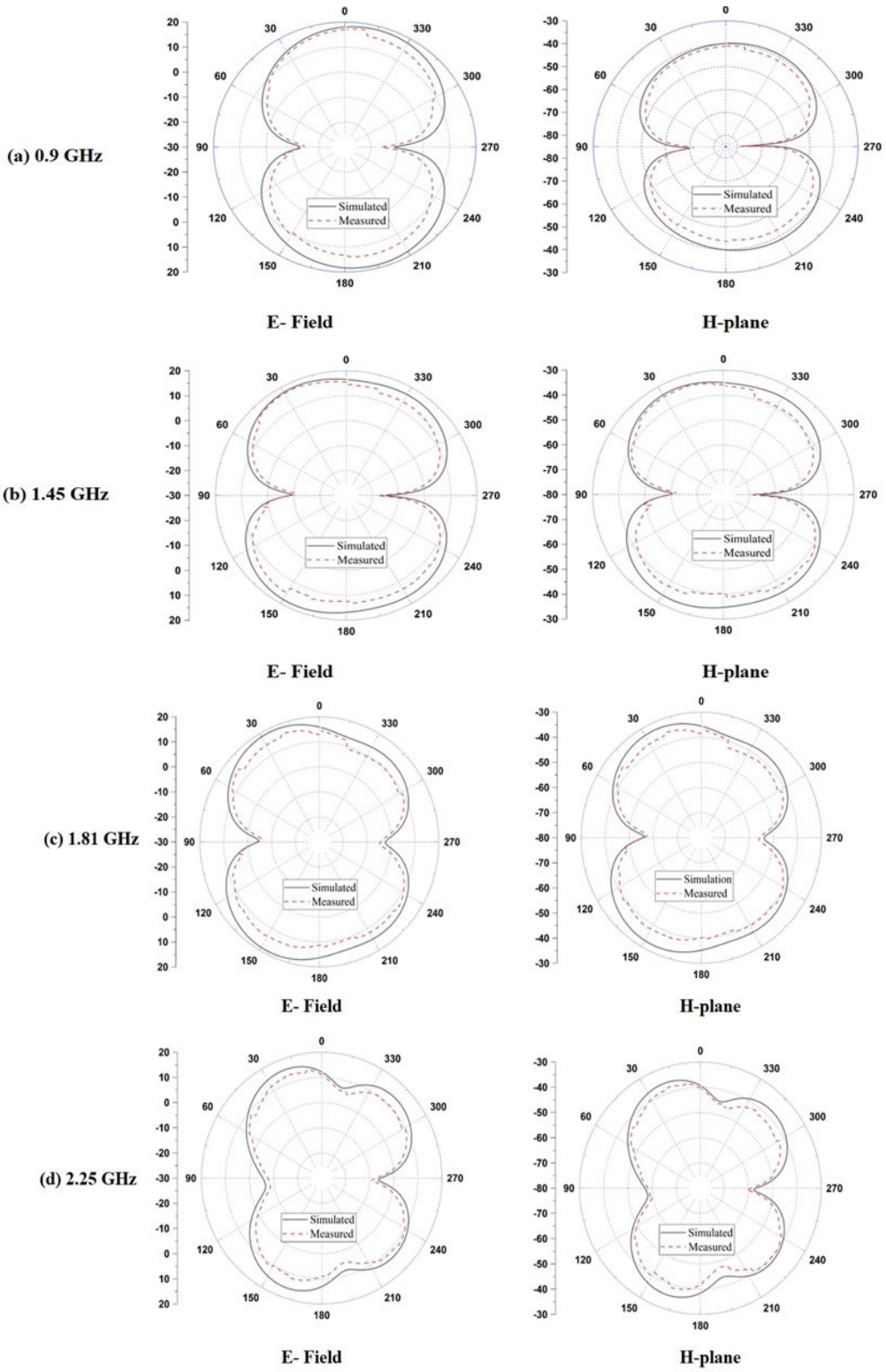

FIGURE 5. Comparison between simulated & measured E and H-field radiation patterns for the suggested antennas; for (a) 0.9 GHz; (b) 1.45 GHz; (c) 1.81 GHz; (d) 2.25 GHz.

supply the EM energy to form high inductance entire the top of the antenna. The fork shape stub is responsible for the deliberation of supplied EM energy to the topmost radiator of the antenna. Furthermore, the surface current distribution at 0.9 GHz supply better insight on the proposed antenna as the distribution of current fluctuates beside the antenna x-axis

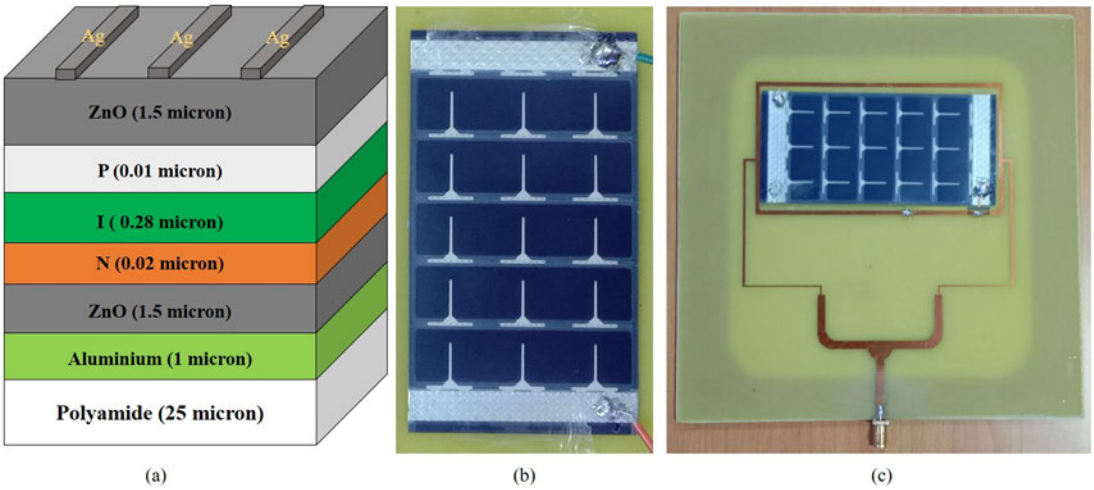

FIGURE 6. Solar power film: (a) constructional details (b) commercial layout (c) placed on top of the antenna.

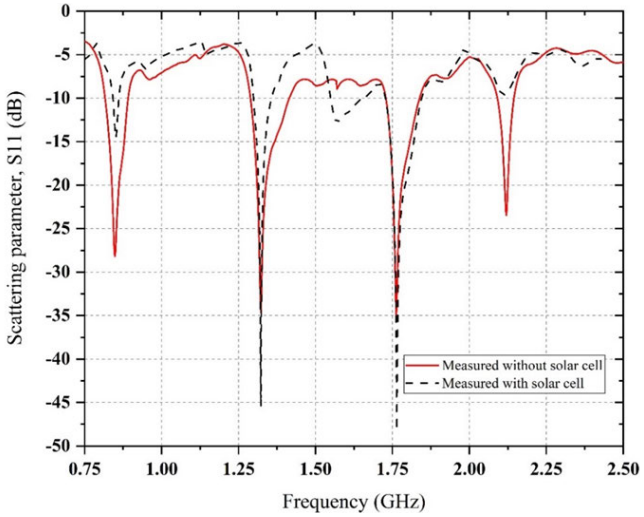

FIGURE 7. Measurement of S-parameter without and with the solar power film of the antenna.

dimension with lower current particles (for frequency bands 0.9 GHz, 1.81 GHz and 2.2 GHz except 1.45 GHz) at the left and right side due to the decreased 'end effect'. Actually, due to the radiation resistance antenna radiates RF energy. These resistance is higher than the loss resistance on the top of the antenna which is typically negligible in the measured results. The maximum current density through the rectangular slot at the top of the antenna is obtained for 0.9 GHz and 1.45 GHz frequency bands whereas the current distribution of 1.81 GHz and 2.25 GHz bands are higher throughout the fork shape or feedline line. The E-field distribution in free space is a measure of how quickly the electric force would be charged per unit area. The electric field (E-field) distributions of the quad-band antenna at different frequency bands are depicted in Figure 10. These results exhibit that maximum E-filed distribution occur around the rectangular slot along with fork shape (i.e. feeding line) and is mainly found at the edges. At devious incidence, it can be seen that the strongest E-field density around rectangular slot along with feeding line at 0.9 GHz than the other frequency bands. The lower electric field distribution are occurred at 1.45 GHz, 1.81 GHz and 2.25 GHz frequency bands. It is evident that electric filed density around the proposed structure is decrease with increase the frequency bands.

Figure 11 ((a) and (b)) shows the comparison of peak realized gain and radiation efficiency of the suggested antenna in terms of the frequency with and without allocated solar cell power film. It can be seen that both gain and efficiency increased due to the integration of the power film solar cell. Thus the antenna gain is increased in the frequency of 1.45 GHz and 1.81 GHz except for the 0.9 GHz and 2.25 GHz. Antenna achieves more than 64% in terms of radiation efficiency for most of the operating frequency bands with solar cell integration. In the case considered, a single solar cell was mounted atop the radiating structure of the antenna. The entire region of the radiating structure may also be occupied by solar cells which can be connected in series or parallel [27]. To do this, it is important to position the required diodes carefully to avoid the problem of reverse currents when there is a discrepancy in the current or the voltage.

V. DESIGN AND IMPLEMENTATION OF QUAD BAND RECTIFIER CIRCUIT

In this research, the rectifier circuit with a voltage doubler configure is proposed for realizing high RF-to-DC rectification efficiency [11], [28]. This simple configuration is more efficient than other complex configurations such as voltage multiplier [29] and Greinacher [30] rectifiers. The schematic of the proposed rectifier is shown in Figure 12. It consists of a matching network, rectifier section and envelope detector. The meander line, short stub and open stubs are part and parcel of the matching circuit whereas an Avago HSMS-2850 model Schottky diode, a 100 pF capacitor and a

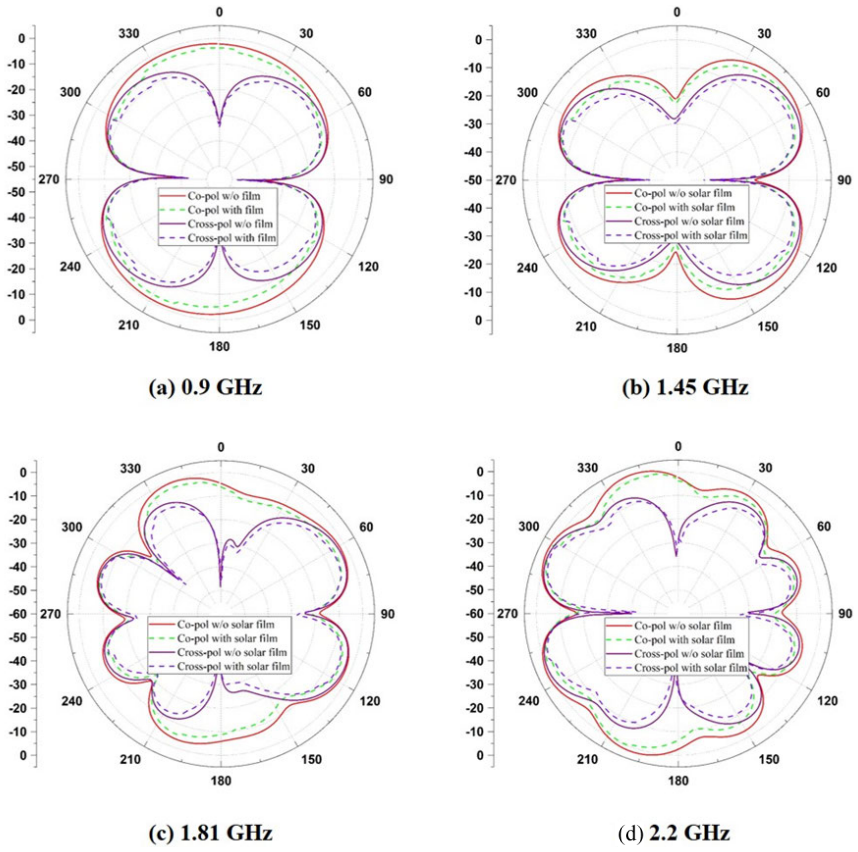

(a) 0.9 GHz (b) 1.45 GHz

(c) 1.81 GHz (d) 2.2 GHz

FIGURE 8. Measurement of directivity of the proposed antenna for different frequency bands (a) 0.98 GHz, (b) 1.45 GHz, (c) 1.81 GHz, and (d) 2.2 GHz with and without solar film.

4.5 kOhm load resistor are elementary components of the RF-to- DC converter section. The HSMS −285B Schottky diode is used due to its high sensitive turn-on voltage, low quiescent current and associated load resistance which is optimized for available ambient RF power level. The 1.6 mm thick FR4 substrate material with 5.4 dielectric components and 0.02 loss tangent is used for the fabrication of the complete rectifier circuit. The Advanced Design System (ADS v 19) of Harmonic-Balance (HB) solver is used to optimize the performance of rectifiers. The nonlinear circuit model of selected diodes with a transmission line (TL) layout is used to ensure high precision with the best performance. The RF-to-DC rectification efficiency of the rectifier defines the amount of dc voltage obtained directly from the RF energy harvester from the ambient level. So, it is essential to ensure the maximum efficiency of the rectifier at the available frequency with an associated RF power level in an ambient environment. To fulfil this goal, it is crucial to set up an optimization process for a wideband antenna which can catch the specified EM signals passed through the matching network to the rectifier and ensure the transfer of maximum power or voltage. To perform combined simulation, the Thevenin equivalent circuit of the antenna (Figure 12) is used with a broadband rectifier to realize harvester operations [31]. The reciprocity formula is used to calculate the open-circuit voltage source (OV) in series with antenna impedance [32] as

$$V_{oc}(\theta_0, \phi_0, S) = \frac{4\pi}{jk\eta_0}(F\theta_0, \phi_0)E_0(S) \tag{1}$$

$$E_0(S) = \sqrt{2\eta_0 S} \tag{2}$$

where $F(\theta_0, \phi_0)$ is the antenna far-field properties, E_0 is the electric field of incoming EM wave to the center of the antenna, S is the Poynting vector of the plane wave and $\eta_0 = 120\pi$ is free space constant. The RF–to-DC rectification efficiency of RF energy harvester is calculated by

$$\eta = \frac{V_{dc}^2}{P_{RF@input} \cdot R_L} \tag{3}$$

$$P_{RF@input} = \frac{|V_{oc}|^2}{8.\mathrm{Re}(Z_A)} \tag{4}$$

where, $p_{RF@input}$ is the ambient RF power, and $\mathrm{Re}(Z_A)$ is the real part of antenna complex impedance.

The impedance matching network (IMN) is a crucial and challenging part of this design. Due to the non-linear behavior of the rectifier, the input impedance of the rectifier varies with the frequency, input power level and load resistance. The IMN is designed to transfer the maximum power from the source to load. The IMN can increase the voltage gain before the RF rectifier to dominate the threshold voltage as

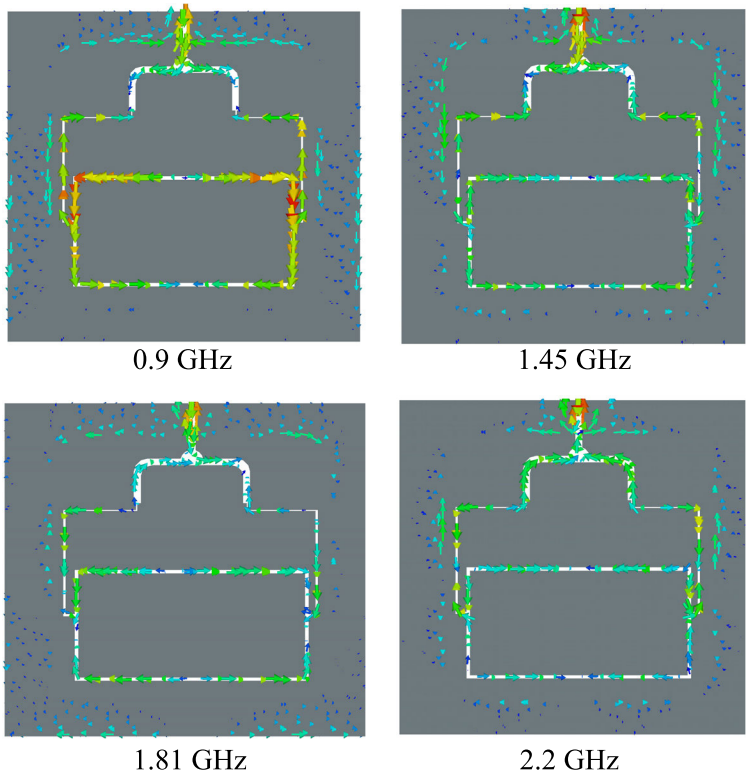

FIGURE 9. The surface current distribution at different frequency bands of the proposed. antenna.

a result of increasing the RF to DC rectification efficiency. Different from the conventional rectenna design for a fixed frequency and input RF power density level, the rectifying element for energy harvesting needs to adapt to the variable conditions of the ambient input signal. The impedance needs to be matched not only as a function of the frequency but also as a function of the input power level. The different type of rectifying elements such as two transmission lines, one short stub and one open stub which consist of the IMN, is aimed to get the circuit matched to the frequency band 0.9 GHz within the frequency range of 0.5 to 2.4 GHz. Similarly, one meander line and two transmission lines for 1.33 GHz, two transmission lines and open stubs for 1.81 GHz, and one transmission line and two open stubs for 2.20 GHz are designed respectively.

The final design is produced for the −20 dBm input power with input impedance of 0.408 +j1.610 @ 0.9 GHz, 4.330+j0.457 @ 1.33 GHz, 1.095+j0.758 @1.81 GHz and 3.244+j0.384@ 2.2 GHz are shown in Figure 15. At the specific operating frequency range, the impedance between source and load are matched in such a way that complex impedances are conjugate to each other. The initial stage in the design of an impedance matching network is to determine the rectifier input impedance of the load section to be fully adapted to the antenna output impedance (source), usually 50 Ω. There are two ways to design IMN such as using lumped components (i.e. inductor and capacitor) and distributed microstrip components (i.e. open stub, short stub, and mender line etc.) respectively. In this research, microstrip matching elements (i.e. second options) are used to design the IMN because they are able to perform maximum power from the source to load. Moreover, the quality factor (Q-factor) of such a type of matching network boosts the threshold voltage level and offers the passive and strong amplification of the RF input signal. The selected IMN topology for the quad-band design is created by stepped connection (both series and parallel) along with various matching elements as shown in Figure 13. After connecting the specific number of microstrip elements for a particular frequency band, the different parametric values (i.e. length, width, and angle) are optimized to achieve the goals which are stated in equation (5). It may enlarge the compound impedance matching network which causes losses. The loss in the IMN may be little but it is comparable with the obtained power from the energy sources. Thus, the loss will lead to a low conversion efficiency as well as impedance bandwidth. When the source output resistance equals the input resistance, the output power is maximum according to the maximum power transfer theory. An impedance matching network realizes maximum power transfer by decreasing the loss during power transformation. Moreover, a less stable RF ground for the impedance network can cost extra loss. High frequency in combination with high inductive and capacitive values (i.e. open stubs and short stubs) are often problematic but can also

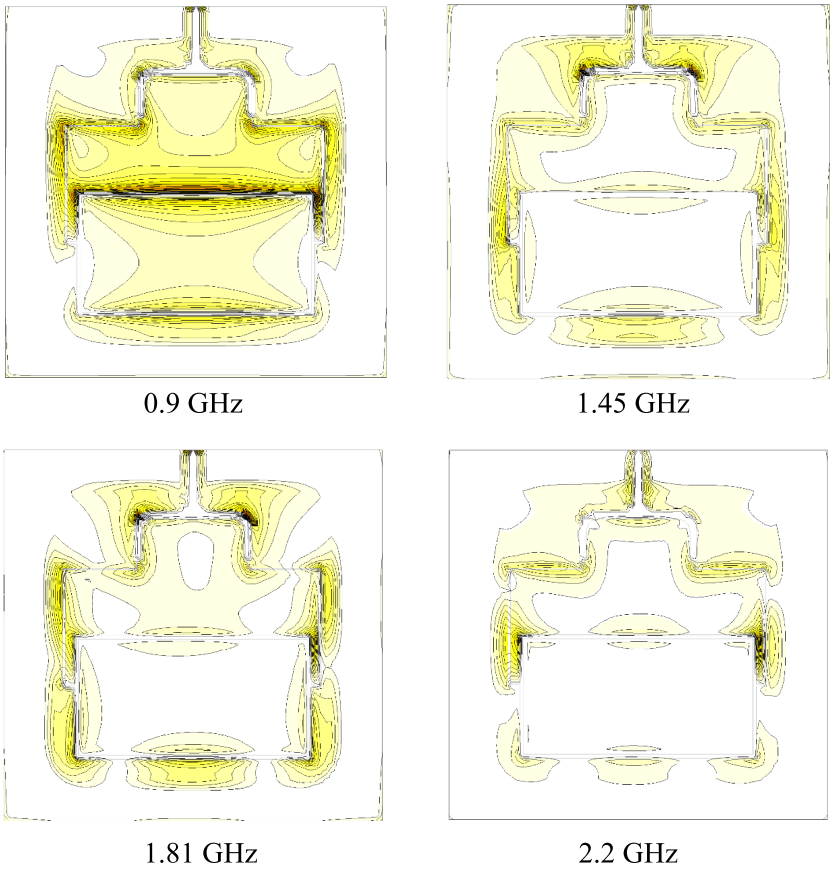

FIGURE 10. The electric field distributions at different frequency bands of the proposed antenna.

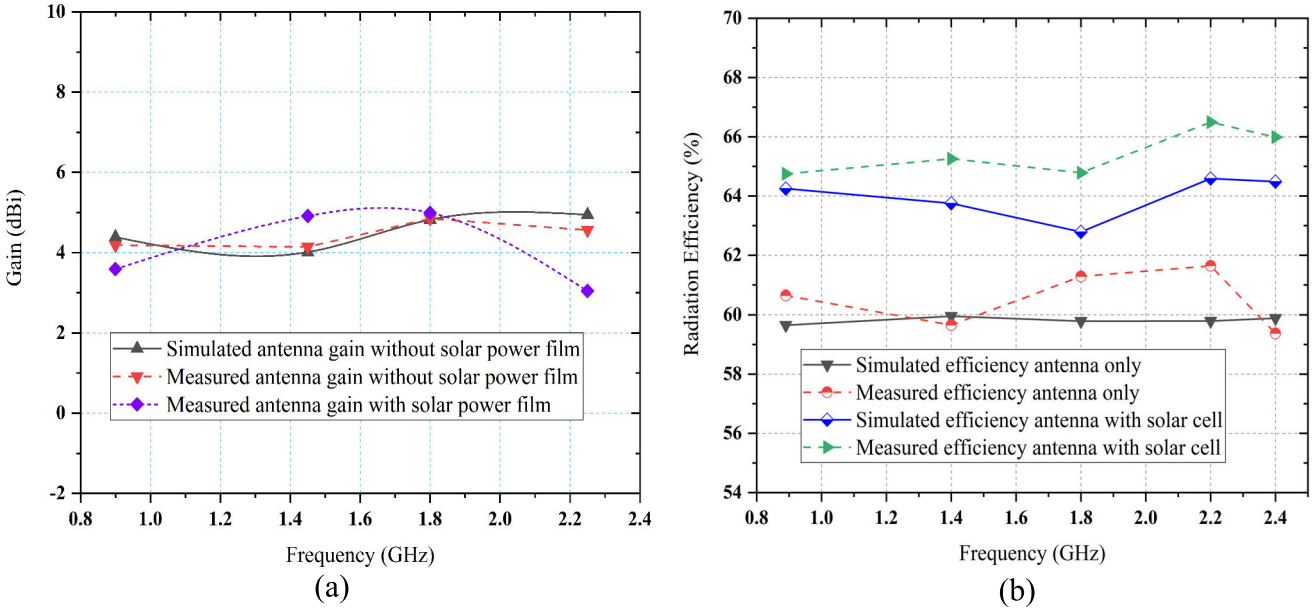

FIGURE 11. Comparison between simulated and measured (a) peak realized gain (b) radiation efficiency of the antenna along with different frequency bands with and without the solar power film.

be turned into an advantage. Some losses are acceptable at a center frequency that can improvements be reached at band-edges, but it is a poor solution as it results in an increased average over bandwidth loss. For total best-optimized result must matching network be included as a part of complete rectifier design from a very early stage. That makes it possible

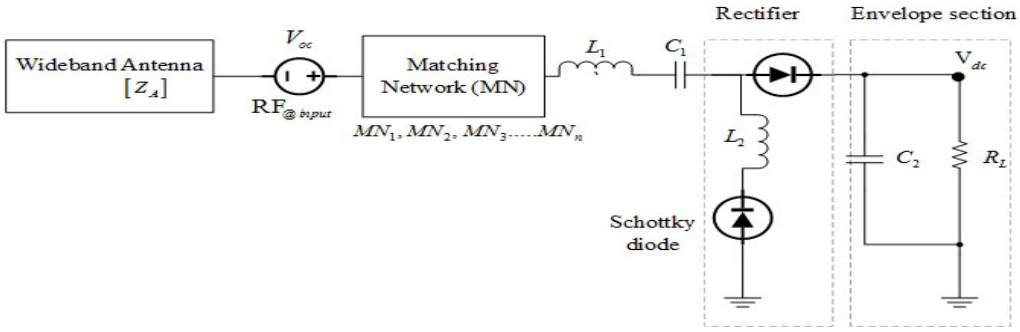

FIGURE 12. The voltage doubler rectifier topology.

TABLE 4. The optimized dimension of different parameters of the proposed rectifier.

Rectifying element	Length (L) mm	Wide (W) mm	Rectifying element	Length (L) mm	Wide (W) mm
TL1	10	2.3125	MLOC3	7.975	1
MLSC	8.9	1.2858	TL6	6.475	1.53875
TL2	20.25	1.5	MLOC4	3.75	1.75
MLOC1	6.8625	1	MLOC5	3.37125	1.53875
TL3	4.125	1.53875	TL7	12.6625	1
MEANDER	68.75	0.9375	TL8	1	1
TL4	9.6581688	1.53875	TL9	3.5	1
MLOC2	6.5875	2.25	TL10	1	1
TL5	14.975	1.53875	TL11	1	1

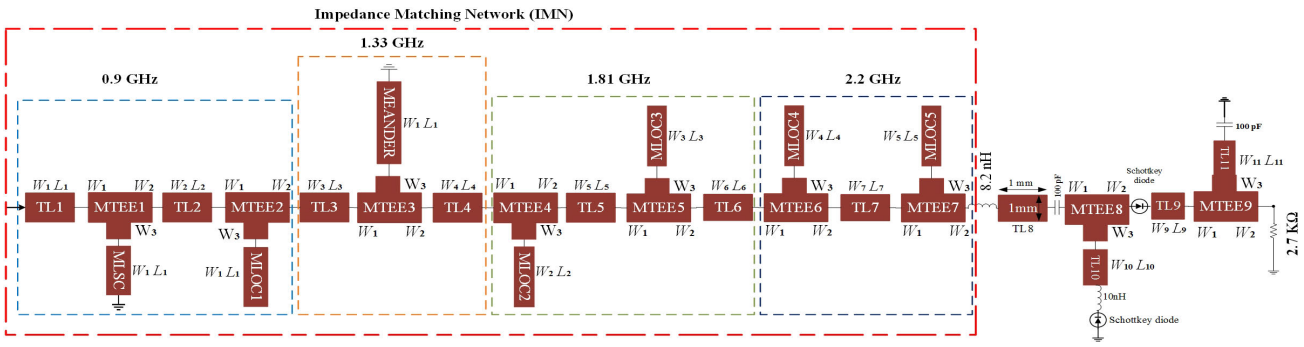

FIGURE 13. The Schematic layout of the proposed wideband quad-band rectifier which operating frequency range 0.9 GHz to 3 GHz.

to get the widest bandwidth with the minimum loss for the network in combination with the antenna, not just the losses for a matching network part.

A similar process is followed before the fulfilment of the total number of frequency bands. The optimized parametric values of various microstrip components are listed in TABLE 4. In this design, the resulting IMN are quad-band MN with better Q-factor with respect to wideband design which is considered in the development the value of DC-rectification efficiency. A Harmonic balance solver of ADS is used to optimize the schematic circuit (Figure 12) and compute the maximum RF-to-DC conversion efficiency with the input of specified frequency bands and associated ambient minimum RF power level. The sequentially addition of different types of microstrip matching elements (i.e. open stub, short stub, and mender line) of the matching network denoted by $ME_1, ME_2, ME_3.....ME_n$ of the rectifier are optimized by performing the tuning operation of schematic of ADS software to get the target frequency bands as well as higher dc rectification efficiency. Also, the optimized value of load resistance is determined by justifying the maximum RF-to-DC efficiency for different values of load resistance. The maximum value of dc rectification efficiency for the corresponding value of load resistance is considered as optimized

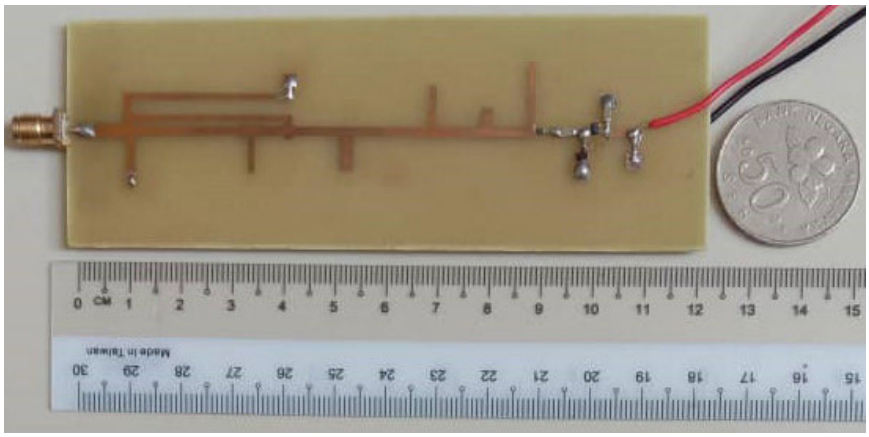

FIGURE 14. The prototype image of the designed rectifier.

load resistance. By the successive iteration process of matching elements, the low value $\eta_{\min}$ is improved until the optimization procedure achieves the higher value of rectification efficiency (η).

If IMN for multiple-frequency are designed, mutual interference arises when the specific resonance frequencies of the separate IMN are near together. The resonance BW will intercede with one another and malfunction will cause if the resonance frequencies of adjacent IMNs are almost together. To decrease this mutual interference, IMN with different resonance frequencies are accessible to slight movement the oscillating or resonance frequencies of the combined IMN. Using an S-parameter block with the simulation results from CST, the characteristic impedance Z_A of the antenna part is determined by the harmonic balance optimization technique of ADS. The optimized dimensions of the rectifying elements (TL1-TL11, MLSC, MLOC1-MLOC5, and MEANDER) as well as the layout of the complete rectifier are shown in Figure 13. TABLE 4 depicts the numerical value of the optimized dimension of various parameters of the rectifier. The prototype image of the proposed rectifier is shown in Figure 14. The Avago HSMS 285B Schottky diode with a low threshold voltage (135mV) is used to design and implement the rectifier circuit. The envelope section of the rectifier consists of a series diode with a shunt capacitor rectifier topology which has higher efficiency than the multi-stage diode rectifier for low-level RF ambient power [33]. Using the general optimization procedure, a novel matching network with single-stage rectifier structures is designed and implemented for the best performance of the solar RF harvester element. The performance of the rectifier mainly depends on the matching network between the antenna element and the load section of rectifier topology. The designated ambient RF power level $RF_{@input}$ improves the performance of the proposed rectifiers is -20 dBm.

VI. PERFORMANCE ANALYSIS OF THE BROADBAND RECTIFIER CIRCUIT

To verify the proposed rectifier, a prototype image (Figure 14) was fabricated. The dimension of the active area

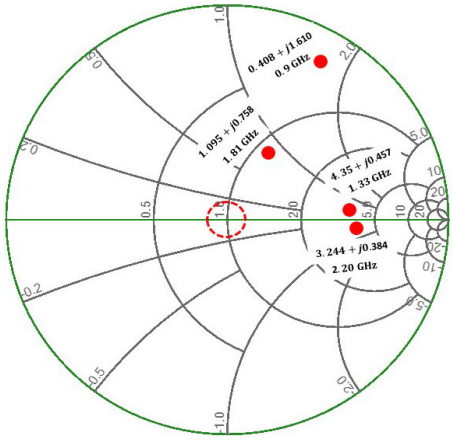

FIGURE 15. The impedance point for each frequency band for the RF input of − 20 dBm.

of the rectifier is 155 mm × 30 mm. The simulated and measured scattering parameter S11 of the rectifier at low RF power input is presented in Figure 16. There is an excellent agreement between measured and simulated S-parameter (S11) of the rectifier because of its new matching network. In Figure 13, there are four resonances at the GSM 900, LTE 1.33 GHz, GSM 1800 and 3G frequency bands and the resonant frequencies have a slight deviation between simulation and measured S11 at −20 dBm RF power. The suggested wideband rectifier can convert the incoming RF signal to DC signal within the range of 0.5 GHz to 2.5 GHz. The new optimization technique is used to achieve the following goal in the ADS simulation process:

$$\begin{aligned} \eta_{RF-to-DC[0.5\ GHz-0.1\ GHz]} &> \eta_{\min} \\ \eta_{RF-to-DC[0.1\ GHz-1.9\ GHz]} &> \eta_{\min} \\ \eta_{RF-to-DC[1.9\ GHz-2.5\ GHz]} &> \eta_{\min} \\ \eta_{RF-to-DC[0.5GHz-2.5GHz]} &> \eta_{RF-to-DC[\min]} \end{aligned} \quad (5)$$

To satisfy this optimization goal, the parametric performance of the impedance matching network between the solar antenna and the wideband rectifier circuit has been optimized and analyzed. The resulting matching network is a wideband

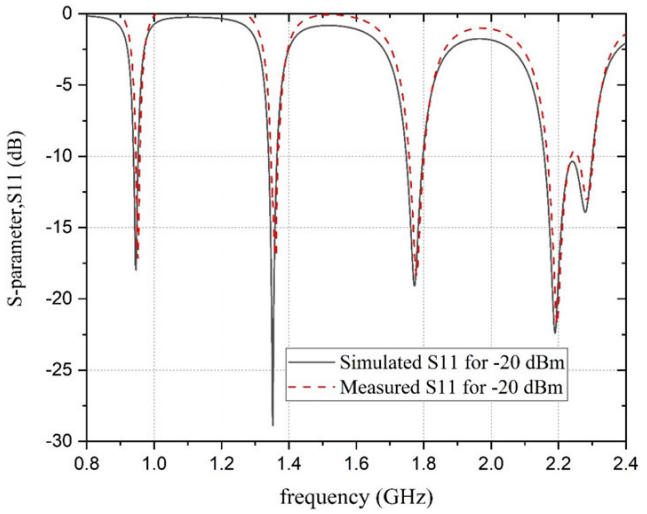

FIGURE 16. Simulated and measured scattering parameter S_{11} of the rectifier at −20 dBm RF power.

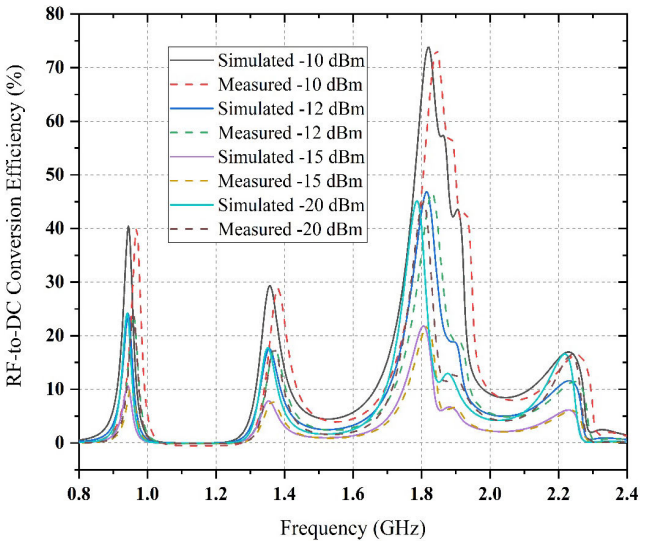

FIGURE 17. The comparison between simulated and measured RF-to-DC rectification efficiency for different ambient power levels.

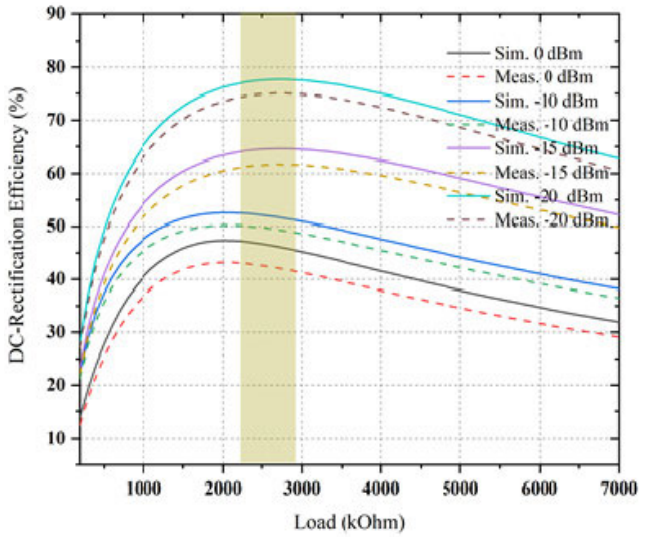

FIGURE 18. The comparison between simulated and measured RF-to-DC rectification efficiency for different ambient power levels with respect to load value.

network (Figure 13) that covers the target resonance frequency bands as well as maximum RF-to-DC rectification efficiency due to its suitable impedance level. The comparison between simulated and measured RF-to-DC rectification efficiency for different RF power levels of the proposed rectifier is presented in Figure 17. The wideband properties of the matching network are enabled to achieve at least 3 dB magnitude of the scattering parameter [34]. It is observed that maximum efficiency achieved at −10 dBm is about 75% whereas minimum efficiency occurs at −15 dBm. Due to the limitation of available ambient RF power level, −20 dBm is acceptable except for other RF power. The comparison between measured and simulated dc conversion efficiency is in good agreement at different frequency bands 24.6%, 17.3%, 46.5% and 12.4% for −20 dBm, respectively, demonstrating excellent dc rectification efficiency for all target frequency bands at available low ambient power. The proposed hybrid rectenna harvests RF energy available all frequency bands between 500 MHz to 2.7 GHz. Figure 18 illustrates the DC rectification efficiency as a function of load resistance for constant input frequency at 0.9 GHz. The optimal load resistance is selected at 2.7 kΩ, because of maximum RF-to-DC rectification efficiency which results of higher output dc voltage of the quad-band rectifier at its corresponding central frequency. The maximum dc-rectification efficiency (i.e. about 78% and 75% simulated and measured values respectively) is achieved at 2.7 kΩ for −20 dBm ambient RF power level.

When the input RF power levels are less than −20 dBm (i.e. not available in ambient power level) then maximum efficiency appeared with the value of load resistance below 2 kΩ. Figure 19 shows the comparison between measured and simulated RF-to-DC rectification efficiencies of the multi-tone input RF frequency signals versus input ambient RF power for every single tone. It is observed that multiple input RF frequency signals increased the RF-to-DC conversion efficiency compared to the single input RF frequency signal. The quad-tone RF input signal (0.9 GHz, 1.33 GHz, 1.81 GHz, and 2.20 GHz) has the maximum RF-to-DC conversion efficiency and can rise the RF-to-DC conversion efficiency by up to 4 times compared to the single input RF signal of −20 dBm ambient RF power level. The higher conversion efficiency means more ambient RF power being absorbed from the broad bandwidth. The overall input RF power is the resultant multiplication of the number of RF signals with the RF power for every single tone. Therefore while having the same RF input power for each tone, the entire RF input power will increase along with the addition of RF tones. Similarly, multiband antennas can receive more RF power compared to single-band antennas due to the scattered RF power across all frequency bands. Consequently, Figure 20 shows the

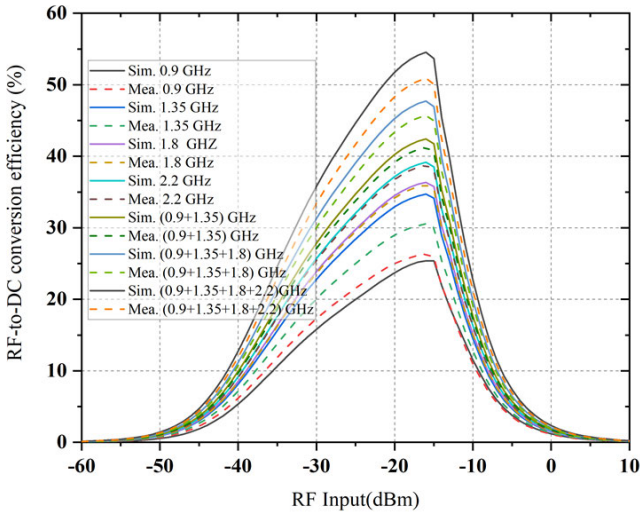

FIGURE 19. Simulated and Measured RF-to-DC conversion efficiency of the quad-band rectifier circuit for various single-tone and multiple input signals for constant RF power level in dBm.

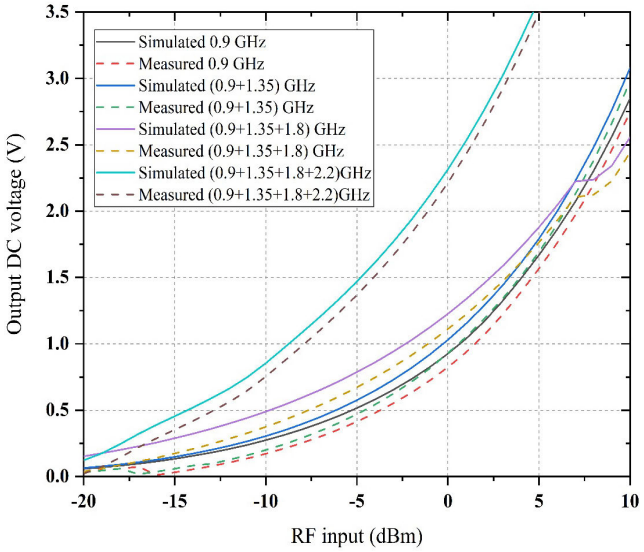

FIGURE 20. Comparison between simulated and measured output dc voltage at quad-band rectifier with respect to the RF input power.

advantage of the quad-band operation in ambient RF energy scavenging in which the RF-to-dc rectification efficiency and the generated dc power can be increased. The generated dc output voltage of the energy harvester not only depends on RF-to-DC rectification efficiency but also input RF power level. Therefore, analysing the performance of hybrid energy harvesting systems contrasted with the ambient RF power density is essential. From Figure 20, it is demonstrated that the proposed hybrid energy harvester scavenges more RF power from multiple signals compared to a single signal and delivers higher dc voltage. The multiple signals (i.e. quad-tone such as 0.9 GHz, 1.33 GHz, 1.81 GHz and 2.25 GHz) have the higher output dc voltage between all cases. The quad-tone RF input signals can generate output dc voltage 1.8 times from dc voltage produced by single-tone

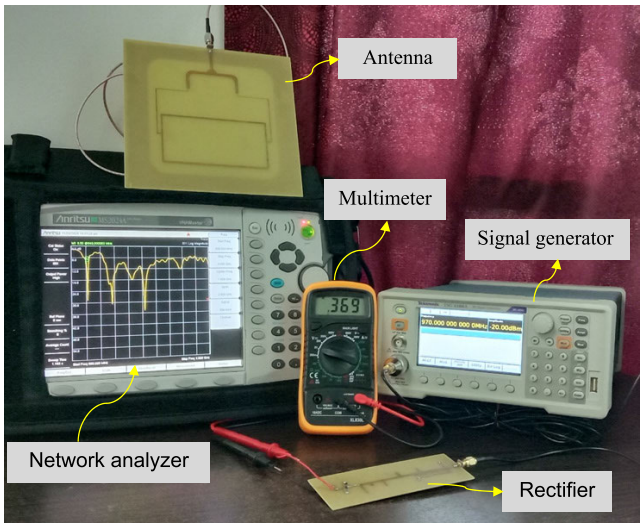

FIGURE 21. The measurement setup in lab.

RF input, depicting the advantage of the quad-band operation of the suggested hybrid energy scavenging system.

VII. EXPERIMENTAL SETUP IN LAB

Figure 21 depicts the measurement setup in lab environment. An Anritsu MS2024A VNA Master handheld Vector Network Analyzer, a TSG4104A RF vector signal generator and a digital multimeter is used to measure the performance of the RF harvester in the applied lab at MMU. To evaluate the competency of the harvesting RF power, we can test the suggested hybrid energy harvesting for different RF power level in the lab environment as depicted in Figure 22. It is observed that the proposed hybrid harvester can produce output dc voltage around 0.395 V (RF harvester) and 0.504 V (Hybrid harvester) as displayed in Figure 22 (a) and 22 (b). The integration of solar cells with antenna increases the generated output dc voltage about 0.109 V more than the RF harvester. In a controlled lab environment, both harvesters are tested to a multimeter and the RF signal generator (APSIN12G, 100 kHz −12 GHz) is set to four different frequencies (0.9 GHz, 1.33 GHz, 1.81 GHz and 2.20 GHz) while associated RF power remains constant at −20 dBm for every single tone. To progress the accuracy of the realistic results, the experiment is conducted several times to check the overall RF-to-DC conversion efficiency as well as output DC voltage generated by the hybrid harvester. As well as expanding the operating range of the passive radio frequency identification (RFID) tag [36], the hybrid energy harvester will greatly increase the total available power available in a device. In addition, the performance of the power conversion of electromagnetic energy found in the solar spectrum to electricity depends on the level of illumination used, the photoactive material used and the design of the system (solar cell power film layer). The output of a photovoltaic device is limited by increased power losses at low indoor irradiance levels (approx. 100 μW cm^{-2}), as the value of the device shunt resistance becomes comparable to that of the

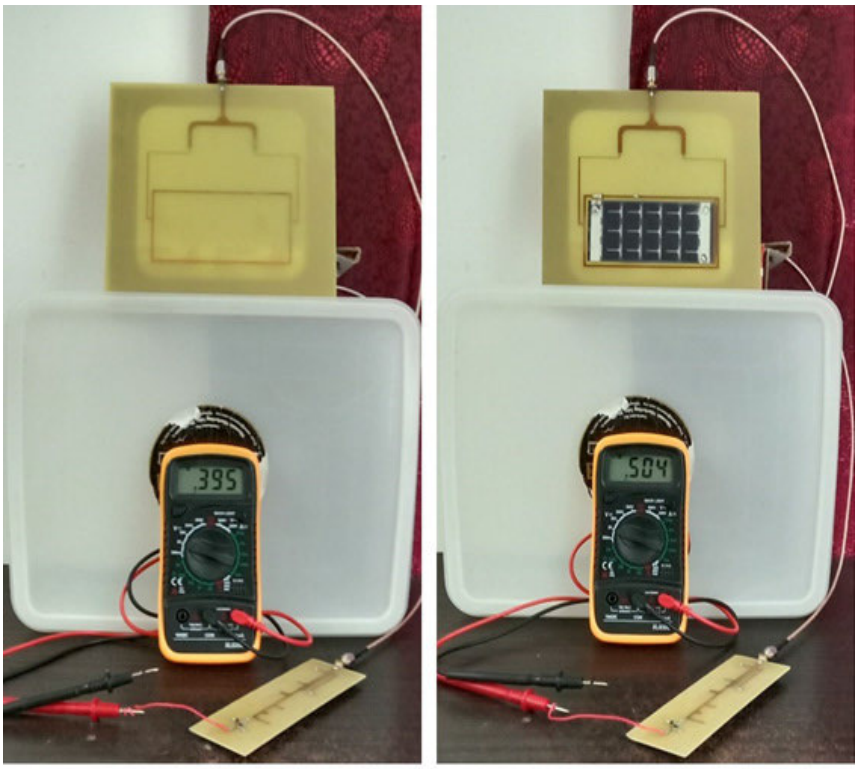

FIGURE 22. Measured output dc voltage (a) without solar cell and (b) with solar cell at quad-band rectifier with respect to the RF input power.

cell's characteristic resistance, defined as the ratio between the open circuit voltage and the short circuit current. The effect of increasing the RF input power level will contribute to the DC performance of the EM harvester is comparable to that of the solar cells in ambient light conditions (low irradiance values). In the case of higher irradiance conditions, the main contribution to the DC voltage comes from the solar cells and the increase in the RF input power level does not substantially reflect the DC voltage obtained. The use of the hybrid solar/EM is more appropriate under low irradiance conditions for low RF input power density levels, whereas the hybrid harvester could just be run as a solar harvester if the irradiance is high. These facts indicate that adding solar cells that produce an almost constant voltage under adequate lighting conditions will allow the ''cold start'' start-up of a dc-dc converter to enable RF energy harvesters to scavenge low-power energy afterwards. At the same time, when solar cells are unable to produce any electricity, RF energy harvesters continuously generate energy during the night time.

VIII. EVALUATION OF HARVESTER PERFORMANCE IN BOTH LAB AND AMBIENT ENVIRONMENT USING BQ-25504 EVM

To realize the cold-start performance of the hybrid harvester, the output of the harvester is connected to a power management module (PMM) BQ-25504 in series, as depicted in Figure 23. It has the dynamic maximum power point tracking (MPPT) properties that help to prevent the collapsing input RF sources with a random variable power level. Moreover, this MPPT dynamically optimizes input RF power source operating point for the extraction of maximum power from available ambient RF sources with associated power levels. The probability of generated output dc voltage on the cold-start PMM input range (300 mV for BQ-25504) beneath any ambient scenario has risen. The PMM circuit can provide efficient acquisition and management of generated voltage with a low level of input RF power as a result of increasing output dc voltage level. The BQ-25504 supports harvesting energy from a variety of ambient energy sources from different frequency ranges associated with very low-level input RF power. Figure 23 shows that the output voltage of the rectifier is passed through the EVM BQ-25504 and the final generated output DC voltage from PMM is about 0.688 V which is more than 0.184 V without EVM. The generated output voltage and current of the BQ-25504 are measured using a multimeter, and the RF-to-DC conversion efficiency is calculated from input and output power. TABLE 5 shows the comparison between several quad-band hybrids harvesters designed for different input frequencies associated with low RF power. Given the elementary similarity in hybrid harvesters of [35], [37] and comparing the above-mentioned performance parameters such as

TABLE 5. Performance comparison between different Hybrid Energy harvesters.

Reference	Source of Energy	Frequency range	Peak Gain (dBi)	Efficiency	Load	Sensitivity
[35]	EM + Solar	0.850 to 6 GHz	3.5 dBi	15%	3.1 KΩ	-17 dBm @ 300 mV
[36]	EM + Solar	2 to 3 GHz	1.9 dBi	30%	1.5 KΩ	-3 dBm @ 1.5 mV
[37]	EM + Solar	2.25 to 2.28 GHz	7.4 dBi	20%	3.5 KΩ	-17 dBm @ 2.8 V
This work	EM + Solar	0.820 to 2.4 GHz	5 dBi	48.2%	2.7 KΩ	-20 dBm @ 0.707V

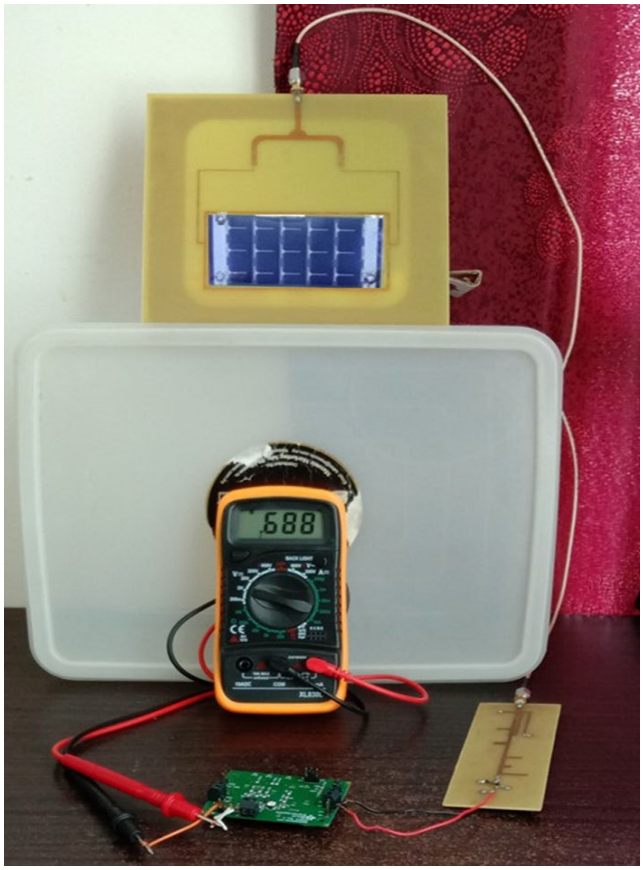

FIGURE 23. Evaluation of Hybrid harvester using the BQ-25504 power management module (PMM).

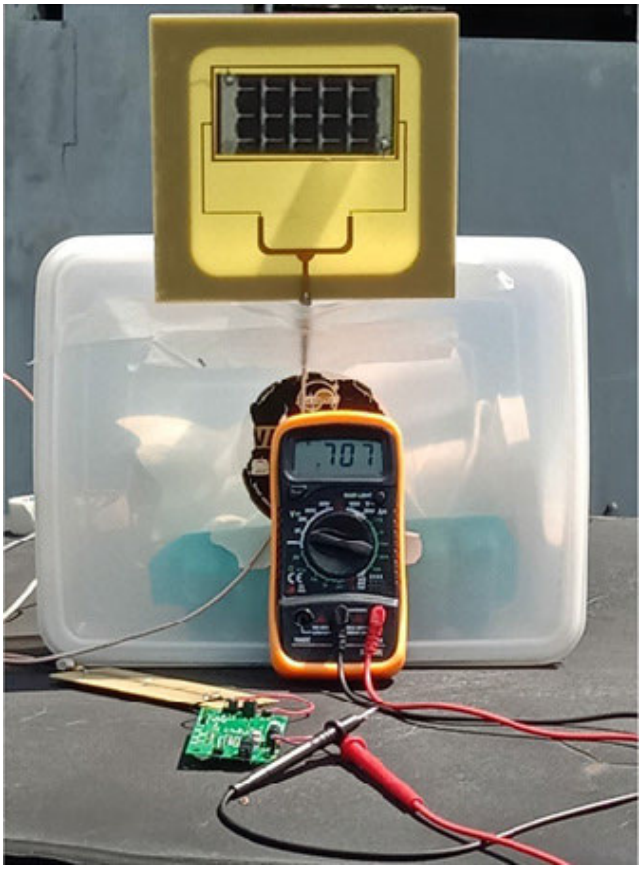

FIGURE 24. The measurement of hybrid harvester in ambient conditions (sunny day).

the antenna gain, RF-to-DC conversion efficiency, load and generated output dc voltage for different RF power levels, it can be demonstrated from TABLE 5 that the suggested hybrid harvester can offer competitive performance. From TABLE 2, solar power is measured by using a solar meter in different ambient temperatures of both sunny and cloudy conditions. So it is demonstrated that in different irradiance conditions, the amount of power harvested is different. From Figure 22 (b), 23 and 24, it is shown that the amount of harvested energy of different irradiance conditions are 0.504 V, 0.688 V and 0.707 V respectively. The light intensity in a dark or night environment is lower than in a sunny environment. The current from the solar cell was varied by changes of the light intensity in various conditions.

Figure 25 shows the generated output dc voltage is 0.405 V in a night environment which is 0.302V lower than the voltage in sunny conditions. The scattering parameter ($|S11|$) increases first as solar current increases, but it decreases if the input current is too large and the solar power is dominant.

Overall, Figure 24 and 23 depict that the proposed hybrid rectenna system can offer an output dc voltage of 0.707 V and 0.688 V in ambient outdoor and indoor environments respectively. Such type of output dc voltage can be used to power up low voltage and small duty-cycle electronics devices such as sensors in internet of things (IoT) [38], [39], [8]. The proposed design has the highest antenna operating bandwidth, highest gain, circular polarization compared with other

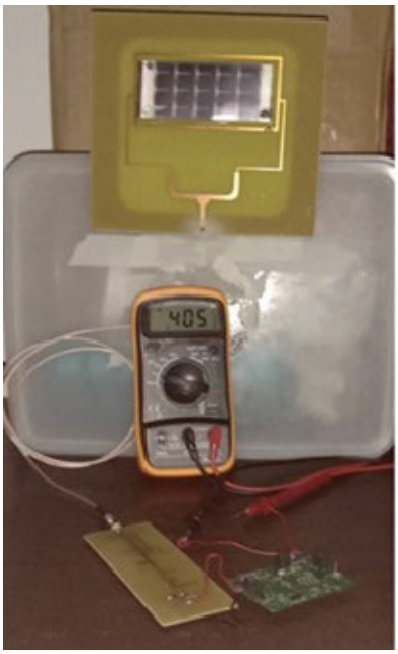

FIGURE 25. The measurement of the hybrid harvester in a dark or night environment.

EM/solar energy harvesters, which is more suitable for environmental RF energy harvesting than linear polarization due to the unknown polarization of the harvested transmitting antennas, and simultaneous wireless communication capability while harvesting ambient energy. Therefore, the suggested hybrid recetenna is assuredly one promising approach to defeat the challenge of battery less device and alternative in IoT.

IX. CONCLUSION

This manuscript covers the area of hybrid energy scavenging in which both the electromagnetic and solar energy sources are considered to use in an ambient environment where the input RF frequencies are available with associated power levels. The key importance of this harvester is the sharing of solar cell power film with the same radiating area of the proposed antenna, which in effect minimizes the size of the complete harvester. This work also covers the solar to EM converters where solar energy is utilized to energize frequency generation circuits that synthesize EM signals to be used as wireless power transmitters. Moreover, the use of rectifier topologies that minimize their sensitivity to input power and load variations based on the use of RCN are covered in this paper. Finally, the proposed quad-band high-gain wideband hybrid energy scavenging system is implemented and measured in the lab. It is ensured that the hybrid energy scavenger can produce an output dc voltage of more than 0.707 V in ambient environment and RF-to-DC rectification efficiency of more than 50% at the input RF power level of −20 dBm. It is also demonstrated that the prototype hardware can provide equal or more output dc voltage both in outdoor and indoor environments, respectively. The suggested hybrid energy harvester could find various applications in IoT, smart skin sensors and machine-to-machine (M2M) applications in rough operation environments.

REFERENCES

[1] V. C. Gungor and G. P. Hancke, "Industrial wireless sensor networks: Challenges, design principles, and technical approaches," *IEEE Trans. Ind. Electron.*, vol. 56, no. 10, pp. 4258–4265, Oct. 2009.

[2] R. Vyas, V. Lakafosis, A. Rida, N. Chaisilwattana, S. Travis, J. Pan, and M. M. Tentzeris, "Paper-based RFID-enabled wireless platforms for sensing applications," *IEEE Trans. Microw. Theory Techn.*, vol. 57, no. 5, pp. 1370–1382, May 2009.

[3] L. Atzori, A. Iera, and G. Morabito, "The Internet of Things: A survey," *Comput. Netw.*, vol. 54, no. 15, pp. 2787–2805, Oct. 2010.

[4] C. R. Farrar and K. Worden, "An introduction to structural health monitoring," *Phil. Trans. Roy. Soc.*, vol. 365, pp. 303–315, Dec. 2007.

[5] L. Gao, Y. Zhang, V. Malyarchuk, L. Jia, K.-I. Jang, R. C. Webb, H. Fu, Y. Shi, G. Zhou, L. Shi, D. Shah, X. Huang, B. Xu, C. Yu, Y. Huang, and J. A. Rogers, "Epidermal photonic devices for quantitative imaging of temperature and thermal transport characteristics of the skin," *Nature Commun.*, vol. 5, no. 1, pp. 38–49, Sep. 2014.

[6] S. Priya and D. J. Inman, *Energy Harvesting Technologies*. New York, NY, USA: Springer, 2009, doi: 10.1007/978-0-387-76464-1.

[7] W. C. Brown, "The history of power transmission by radio waves," *IEEE Trans. Microw. Theory Techn.*, vol. MTT-32, no. 9, pp. 1230–1242, Sep. 1984.

[8] J. A. Hagerty, F. B. Helmbrecht, W. H. McCalpin, R. Zane, and Z. B. Popovic, "Recycling ambient microwave energy with broad-band rectenna arrays," *IEEE Trans. Microw. Theory Techn.*, vol. 52, no. 3, pp. 1014–1024, Mar. 2004.

[9] R. J. Vyas, B. B. Cook, Y. Kawahara, and M. M. Tentzeris, "E-WEHP: A battery less embedded sensor-platform wirelessly powered from ambient digital-TV signals," *IEEE Trans. Microw. Theory Techn.*, vol. 61, no. 6, pp. 2491–2505, Jun. 2013.

[10] J. Bito, J. G. Hester, and M. M. Tentzeris, "Ambient RF energy harvesting from a two-way talk radio for flexible wearable wireless sensor devices utilizing inkjet printing technologies," *IEEE Trans. Microw. Theory Techn.*, vol. 63, no. 12, pp. 4533–4543, Dec. 2015.

[11] S. Shen, C.-Y. Chiu, and R. D. Murch, "Multiport pixel rectenna for ambient RF energy harvesting," *IEEE Trans. Antennas Propag.*, vol. 66, no. 2, pp. 644–656, Feb. 2018.

[12] C. Alippi and C. Galperti, "An adaptive system for optimal solar energy harvesting in wireless sensor network nodes," *IEEE Trans. Circuits Syst. I, Reg. Papers*, vol. 55, no. 6, pp. 1742–1750, Jul. 2008.

[13] S. Beeby and N. White, *Energy Harvesting for Autonomous Systems*. Norwood, CA, USA: Artech House, 2010.

[14] J. McCullagh, "An active diode full-wave charge pump for low acceleration infrastructure-based non-periodic vibration energy harvesting," *IEEE Trans. Circuits Syst. I, Reg. Papers*, vol. 65, no. 5, pp. 1758–1770, May 2018.

[15] D. R. Myers, K. Emery, and C. Gueymard, "Revising and validating spectral irradiance reference standards for photovoltaic performance evaluation," *J. Sol. Energy Eng.*, vol. 126, no. 1, pp. 567–574, Feb. 2004.

[16] M. Green, *Third Generation Photovoltaics, Advanced Solar Energy Conversion*. Berlin, Germany: Springer-Verlag, Dec. 2006.

[17] D. Brunelli, C. Moser, L. Thiele, and L. Benini, "Design of a solar-harvesting circuit for battery less embedded systems," *IEEE Trans. Circuits Syst.*, vol. 56, no. 11, pp. 2519–2528, Nov. 2009.

[18] M. Danesh and J. R. Long, "Photovoltaic antennas for autonomous wireless systems," *IEEE Trans. Circuits Syst. II, Exp. Briefs*, vol. 58, no. 12, pp. 807–811, Dec. 2011.

[19] W. C. Brown, R. H. George, and N. I. Heeman, "Microwave to DC converter," U.S. Patent 3 434 678, Feb. 3, 1969.

[20] A. Upson, "Putting wireless to work," *IEEE Spectr.*, vol. 45, p. 63, Jun. 2008.

[21] F. Declercq, A. Georgiadis, and H. Rogier, "Wearable aperture-coupled shorted solar patch antenna for remote tracking and monitoring applications," in *Proc. 5th Eur. Conf. Antennas Propag. (EUCAP)*, Apr. 2011, pp. 2992–2996.

[22] J.-P. Curty, N. Joehl, F. Krummenacher, C. Dehollain, and M. J. Declercq, "A model for -power rectifier analysis and design," *IEEE Trans. Circuits Syst. I, Reg. Papers*, vol. 52, no. 12, pp. 2771–2779, Dec. 2005.

[23] J. Yi, W.-H. Ki, and C.-Y. Tsui, "Analysis and design strategy of UHF micro-power CMOS rectifiers for micro-sensor and RFID applications," *IEEE Trans. Circuits Syst. I, Reg. Papers*, vol. 54, no. 1, pp. 153–166, Jan. 2007.
[24] M. R. Ghaderi and F. Mohajeri, "A compact hexagonal wide-slot antenna with microstrip-fed monopole for UWB application," *IEEE Antennas Wireless Propag. Lett.*, vol. 10, pp. 682–685, Sep. 2011.
[25] S. Vaccaro, J. R. Mosig, and P. de Maagt, "Two advanced solar antenna 'SOLANT' designs for satellite and terrestrial communications," *IEEE Trans. Antennas Propag.*, vol. 51, no. 8, pp. 2028–2034, Aug. 2003.
[26] A. V. Shah, H. Schade, M. Vanecek, J. Meier, E. V. Sauvain, N. Wyrsch, U. Kroll, C. Droz, and J. Bailat, "Thin-film silicon solar cell, technology," *Prog. Photovolt*, vol. 12, pp. 113–142, Apr. 2004.
[27] M. Tanaka, R. Suzuki, Y. Suzuki, and K. Araki, "Microstrip antenna with solar cells for microsatellites," in *Proc. IEEE Int. Symp. Antennas Propag. (AP-S)*, vol. 2, Jun. 1994, pp. 786–789.
[28] S. Shen, C.-Y. Chiu, and R. D. Murch, "A dual-port triple-band L-probe microstrip patch rectenna for ambient RF energy harvesting," *IEEE Antennas Wireless Propag. Lett.*, vol. 16, pp. 3071–3074, Oct. 2017.
[29] T. Peter, T. A. Rahman, S. W. Cheung, R. Nilavalan, H. F. Abutarboush, and A. Vilches, "A novel transparent UWB antenna for photovoltaic solar panel integration and RF energy harvesting," *IEEE Trans. Antennas Propag.*, vol. 62, no. 4, pp. 1844–1853, Apr. 2014.
[30] C. Song, Y. Huang, J. Zhou, J. Zhang, S. Yuan, and P. Carter, "A high efficiency broadband rectenna for ambient wireless energy harvesting," *IEEE Trans. Antennas Propag.*, vol. 63, no. 8, pp. 3486–3495, Aug. 2015.
[31] J. Mautz and R. Harrington, "Modal analysis of loaded N-port scatterers," *IEEE Trans. Antennas Propag.*, vol. 21, no. 2, pp. 188–199, Mar. 1973.
[32] R. E. Collin, *Antennas and Radio Wave Propagation*. New York, NY, USA: McGraw-Hill, 1985.
[33] A. Georgiadis, G. V. Andia, and A. Collado, "Rectenna design and optimization using reciprocity theory and harmonic balance analysis for electromagnetic (EM) energy harvesting," *IEEE Antennas Wireless Propag. Lett.*, vol. 9, pp. 444–446, Sep. 2010.
[34] M. P. David, *Microwave Engineering*, 3rd. New York, NY, USA: Wiley, 2004.
[35] A. Collado and A. Georgiadis, "Conformal hybrid solar and electromagnetic (EM) energy harvesting rectenna," *IEEE Trans. Circuits Syst. I, Reg. Papers*, vol. 60, no. 8, pp. 2225–2234, Aug. 2013.
[36] K. Niotaki, F. Giuppi, A. Georgiadis, and A. Collado, "Solar/EM energy harvester for autonomous operation of a monitoring sensor platform," *Wireless Power Transf.*, vol. 1, no. 1, pp. 44–50, Mar. 2014.
[37] J. Bito, R. Bahr, J. G. Hester, S. A. Nauroze, A. Georgiadis, and M. M. Tentzeris, "A novel solar and electromagnetic energy harvesting system with a 3-D printed package for energy efficient Internet-of-Things wireless sensors," *IEEE Trans. Microw. Theory Techn.*, vol. 65, no. 5, pp. 1831–1842, May 2017.
[38] A. E. Abdulhadi and R. Abhari, "Multiport UHF RFID-tag antenna for enhanced energy harvesting of self-powered wireless sensors," *IEEE Trans. Ind. Informat.*, vol. 12, no. 2, pp. 801–808, Apr. 2016.
[39] V. Kuhn, C. Lahuec, F. Seguin, and C. Person, "A multi-band stacked RF energy harvester with RF-to-DC efficiency up to 84%," *IEEE Trans. Microw. Theory Techn.*, vol. 63, no. 5, pp. 1768–1778, May 2015.

SUNANDA ROY (Graduate Student Member, IEEE) received the B.Sc. degree in electronic and communication engineering (ECE) and the M.Eng. degree in electrical and electronic engineering (EEE) from Khulna University and the Khulna University of Engineering and Technology (KUET), Bangladesh, respectively. He is currently pursuing the Ph.D. degree under the TM Research and Development Research Grant with the Faculty of Engineering (FOE), Multimedia University (MMU), Malaysia. His research interests include ambient RF energy harvesting, hybrid harvesting, MIMO, multiband antenna design, integrated circuit design, and amplifier design.

JUN-JIAT TIANG received the degree in electronics engineering from Multimedia University, Malaysia, the master's degree from the University of Science, Malaysia, and the Ph.D. degree from the Universiti Kebangsaan Malaysia (UKM). He is currently the Senior Lecturer and a Researcher with the Faculty of Engineering, Multimedia University. His research interests include RFID, microwave circuits, antenna, and propagation. He was awarded Gold Medal at the 23rd International Invention, Innovation, and Technology Exhibition (ITEX) 2012, Kuala Lumpur, Malaysia, in May 2012. He has also the received Silver Medal at the Malaysian Technology Expo (MTE) 2013, Kuala Lumpur, Malaysia, in February 2013. He has vast experience while working as a Project Leader in various research grants, such as TM Research and Development from 2019 to 2020, TM Research and Development from 2017 to 2019, Research Grant, Ministry of Science, Technology and Innovation (MOSTI) from 2008 to 2010, and research grant Mini Fund in 2016. He was worked as an Electronics Engineer with the Global Technology Development Group, Motorola Technology Sdn. Bhd., Penang, Malaysia, from May 2006 to May 2007, and Design Automation Engineer with Chipset Structural Design Team, Intel Microelectronics (M) Sdn. Bhd., Pulau Pinang, Malaysia, from September 2004 to July 2005.

MARDENI BIN ROSLEE (Senior Member, IEEE) is currently working as an Associate Professor under the Research Institute of Digital Connectivity and the Faculty of Engineering, Multimedia University, Cyberjaya, Malaysia. He is also the President of MMU Mesra and the Chairman of the Centre of Wireless Technology. At international level, he is the Chairman of Malaysia IEEE Comsoc/VTS and the Head of the Malaysian Radar and Navigations Interest Group (MyRaN ig), Malaysian Society for Engineering and Technology (MY SET), which is for recognized and selected members in professional organization, networking, and interaction with like-minded multidisciplinary professionals from public and private sectors, as well as the international platforms in the 21st century. He also the Chief Executive Officer (CEO), the Founder of Armada Ltd., company. He is a registered Chartered Engineer with Engineering Council U.K., and a member with The Institution of Engineering and Technology (IET), U.K. As a Chartered Engineer, he bring a diversified range of engineering experience in design an development and engineering management. His experiences include the consultation, professional institution, and academic sectors. His current research interests include 5G/6G telecommunication, D2D, satellite, the Internet of Things, and radar communication. At national and international level, he has been involved in industry consultation and collaborations with some companies, private, and government sectors. At national and international level, he has been involved in industry consultation with some companies, such as TM, Celcom, Webe Digital, TM, FCE Nigeria, Tashmanbet Bagdat Erlanuly, Kazakhstan, Mimos Bhd, Sony EMCS, Plexus Sdn Bhd, Aexio Sdn Bhd, MDEC, Innocrest Enterprise, Ministry of Housing and Local Government, MAMPU, and WCC Telco. Besides, he has been invited by IEEE international conference as a the Session Chair, such as in Thailand, China, Japan, South Korea, Australia, and Turkey. He has hold some international conference committees, such as Conference Co-Chair of IEEE MICC2019, committees for IEEE ISTT18, IEEE MICC17, IEEE ISTT16, TPC of IEEE MENACOMM'19 Bahrain, IEEE PIMRC 2019 Turkey, IEEE PIMRC 2018 Italy, IEEE PIMRC 2017 Canada, IEEE PIMRC 2016 Spain, and IEEE PIMRC 2015 Hong Kong. He is the Keynote Speaker of IEEE SOFTT19 and I3CPE'19. His contributions to academic and the engineering professional more than the years have earned him recognitions nationally and internationally, he has awarded 26 international/local awards, including the University Excellent Researcher Award for 2016 and 2018, respectively, a recipient of VTS Chapter of the Year Award, 2017 IEEE 86th VTC2017-fall, 25 September 2017 from Toronto, Canada, the Excellence in European Creativity Special Award 2018, and the World Invention Special Award 2019.

MD TANVIR AHMED (Student Member, IEEE) received the B.Eng. degree from Multimedia University, Cyberjaya. He researched at the Advanced EM Laboratory, Multimedia University. He has been an IEEE Student Member from the very beginning of his undergraduate degree and has co-organized more than 30 workshops, industrial tours, and webinars under the banner of the IEEE MMU Student Branch. He has also worked as the SECRETARIAT of the IEEE Malaysia Annual General Meeting 2018. He is currently working as an Engineer Intern with ABB Malaysia. Throughout his academic life, he received four prestigious Government MERIT Scholarship along with several awards for outstanding academic performances. His research interests include multiband antenna, RF energy harvesting, hybrid energy harvesting, solar, embedded IoT, and machine learning.

M. A. PARVEZ MAHMUD received the B.Sc. degree in electrical and electronic engineering and the M.Eng. degree in mechatronics engineering. After the successful completion of his Ph.D. degree with multiple awards, he worked as a Postdoctoral Research Associate and an Academic with the School of Engineering, Macquarie University, Sydney, NSW, Australia. He is currently an Alfred Deakin Postdoctoral Research Fellow with Deakin University. He worked with the World University of Bangladesh as a Lecturer for more than two years and with the Korea Institute of Machinery and Materials (KIMM) as a Researcher for about three years. His research interests include energy sustainability, secure energy trading, microgrid control and economic optimization, machine learning, data science, and micro/nanoscaled technologies for sensing and energy harvesting. He accumulated experience and expertise in machine learning, life cycle assessment, sustainability and economic analysis, materials engineering, microfabrication, and nanostructured energy materials to facilitate technological translation from the lab to real-world applications for the better society. He has produced more than 115 publications, including one authored book, nine book chapters, 55 journal articles, and 39 fully refereed conference papers. He received several awards, including the Macquarie University Highly Commended Excellence in Higher Degree Research Award 2019. He was involved in teaching engineering subjects in the electrical, biomedical, and mechatronics engineering courses at the School of Engineering, Macquarie University, for more than two years. He is currently involved in the supervision of eight Ph.D. students with Deakin University. He is also a Key Member of the Deakin University's Advanced Integrated Microsystems (AIM) Research Group. Apart from this, he is actively involved with different professional organizations, including Engineers Australia and IEEE.